Brabender®

Polymer Processing Solutions

Twin Screw and Single Screw Applications

MetaStation 4E
Tabletop Drive Unit

TwinLab C
Standalone Twin Screw

Advantages:

- **Small sample sizes for multiple tests per day**
- **Clamshell barrel and segmented screw designs**
- **Small laboratory footprint**

follow us

Brabender®
5-Star Service

Received: 30 April 2020 | Revised: 24 February 2021 | Accepted: 25 February 2021

DOI: 10.1002/pc.26014

RESEARCH ARTICLE

Polymer COMPOSITES WILEY

Modeling of the resin transfer molding process including viscosity dependence with time and temperature

Laisa Luiz Soares[1] | **Sandro Campos Amico**[2] | **Liércio André Isoldi**[1] | **Jeferson Avila Souza**[1]

[1]Universidade Federal do Rio Grande – FURG, Rio Grande, RS, Brazil

[2]Universidade Federal do Rio Grande do Sul – UFRGS, Porto Alegre, RS, Brazil

Correspondence
Jeferson Avila Souza, Universidade Federal do Rio Grande – FURG
Av. Itália km 8 S/N, 96203-900, Rio Grande RS, Brazil.
Email: jasouza@furg.br

Funding information
Conselho Nacional de Desenvolvimento Científico e Tecnológico, Grant/Award Number: 306734/2016-8; Coordenação de Aperfeiçoamento de Pessoal de Nível Superior; Fundação de Amparo à Pesquisa do Estado do Rio Grande do Sul (FAPERGS); Coordenação de Aperfeiçoamento de Pessoal de Nível Superior-Brasil (CAPES)-Finance Code 001; Conselho Nacional de Desenvolvimento Científico e Tecnológico (CNPq)

Abstract

Flow behavior inside the mold cavity of liquid molding processes such as resin transfer molding (RTM) is important information that is necessary to determine filling time and void formation. Most of the studies found in the literature use isothermal models with Newtonian fluids and constant viscosities. However, for some specific applications, the mold filling time dependence on temperature and the viscosity dependence on time and temperature must be considered to precisely predict the flow advance inside the mold. In this study, a viscosity model, that accounts for temperature and time dependence is coupled with a standard computational fluid dynamics (CFD) model to simulate the resin advance inside an RTM mold cavity. The model is simpler than similar methods that describe viscosity as a function of temperature and resin conversion. Nevertheless, the results show that the proposed model is capable of calculating flow advance, air and resin temperatures, and viscosity changes with time and temperature as expected in actual RTM and correlated processing of thick parts or with low injection pressure or high fiber content.

KEYWORDS

numerical simulation, polymeric resin, resin injection, viscosity temperature dependence, viscosity time dependence

1 | INTRODUCTION

Research on composite materials is an important technological issue and many efforts have been applied to this topic. In many manufacturing processes, including liquid injection processes, a polymeric resin is forced to flow throughout a mold cavity previously filled with a reinforcement medium. Examples of such processes are resin transfer molding (RTM) and its variants, such as light-RTM (L-RTM) and vacuum-assisted RTM (VARTM). In these processes, the final quality of the manufactured pieces, in terms of mechanical properties, is highly influenced by the correct specification and control of process parameters such as injection pressure and positioning of inlet/outlet vents. Moreover, control and modeling of the thermophysical properties of the resin and reinforcement medium is also important, thus many studies on resin viscosity[1–3] and reinforcement permeability[4–8] are also found in the literature.

Numerical simulation has been extensively used by researchers to improve the RTM manufacturing process. The results produced from numerical simulations usually show good agreement (qualitative and quantitative) with those of laboratory experiments.[9–13] Due to improvements in computer power and numerical techniques, these solutions are becoming increasingly precise and reliable. The flow behavior inside the mold cavity is determined based on the operating conditions (injection

pressure and geometry) and the physical properties of the resin (viscosity and density) and reinforcement medium (porosity and permeability). Simulation is only trustworthy if all of these parameters are correctly prescribed.

This work focuses on correct the modeling of the resin viscosity. The great majority of the literature considers resin viscosity be constant, which in many cases is actually a good approximation. However, in some applications, the resin viscosity dependence on temperature and cure time must be considered, such as in the infiltration of thick parts with low injection pressure or high fiber content for which the filling time increases.

The curing process in thermoset polymers occurs by gelation and vitrification of the resin. These phenomena alter the physical properties of the resin and affect its rheological behavior. In many applications, a heated mold is used to decrease the resin viscosity and accelerate mold filling. However, this method has an adverse effect on gel time, which may occur before the resin reaches the mold outlet vents.[14,15] In those cases, heat conduction and convection play an important role in resin injection modeling and should be considered in numerical simulations.[16]

Experimental studies[17,18] have demonstrated that high temperature gradients may occur during curing in RTM processing. Due to these gradients, the degree of cure is not homogeneous along the geometry (mold cavity), and residual stresses occur. These residual stresses may affect the mechanical properties of the produced composite. Therefore, it is clear that thermal modeling cannot always be neglected in the numerical modeling of resin injection processes.

Several studies on thermoset polymers have modeled the thermal influence on the viscosity behavior. Two types of models are used in the most common approximation: (a) models in which viscosity varies with temperature and time,[3,19,20] and (b) models in which viscosity depends on the temperature and conversion.[1,21,22] An interesting review of models and parameter estimation techniques can be found in Ref. [2].

In terms of modeling the resin injection process, a nonisothermal model assumes that the viscosity is dependent on temperature and conversion. In these models, fluid flow is solved with either the FE-CV method[12] or the VOF method.[23] Two more transport equations are added to account for the thermal problem: energy and conversion. Examples of this type of modeling include the work of Poodts et al.[24] on the manufacture of a conrod beam via the RTM process. That work includes experimental and numerical modeling and investigates (among other factors), race tracking and, the thermal effect on the flow and mechanical properties of the produced piece. Another nonisothermal three-dimensional (3D) simulation was published by Shi and Dong,[13] who developed their own code based on the VOF method to solve the filling problem and estimate the mold temperature, injection temperature, and internal pressure, with aim of optimizing the process parameters and reducing the mold internal pressure.

Another interesting approach to viscosity variation with time in resin injection processes was considered by Deléglise et al.[25] Those authors considered the fact that the first resin droplet to enter the mold remains there longer than the following droplets and thus, its cure occurs sooner. They explored this idea by analytically and numerically solving two problems: (a) constant flow rate injection and (b) constant pressure injection. An isothermal simulation was performed and the effect of viscosity variation on the pressure gradient and flow front position was investigated.

As shown above, many studies are available on the viscosity dependence of polymeric resins with temperature and conversion, as well as the use of these correlations in a full CFD simulation of the resin injection problem. In the CFD models found in the literature, viscosity is formulated as a function of temperature and conversion. However, this work proposes a different approach in which the viscosity is formulated as a function of temperature and injection time. From the point of view of the complexity of the numerical solution, every new differential equation added to the mathematical formulation considerably increases the simulation efforts (in terms of processing time and convergence). Thus, removing one of these equations substantially simplifies the numerical solution. In this sense, this work aims to simplify the problem by combining the temperature and time effects on the resin advance by changing only the viscosity.

2 | MATERIALS AND METHODS

In RTM, the mold cavity is filled with a reinforcement medium and a polymeric resin is forced through it. This reinforcement is modeled as a porous medium, and the flow is considered incompressible and laminar. In this work, the volume of fluid (VOF) method[23] is used to model the two-phase (air and resin) flow.

In VOF, the fluids are considered immiscible and only one set of momentum and continuity equations are solved for both fluids. The method is formulated with three transport equations[23]:

The continuity equation

$$\nabla \cdot \vec{v} = 0 \tag{1}$$

where, ρ is the density (kg m^{-3}) and $\vec{v}$ is the velocity (m s^{-1}).

The momentum equation

$$\frac{\partial\left(\rho\vec{v}\right)}{\partial t}+\nabla\cdot\left(\rho\vec{v}\,\vec{v}\right)=-\nabla p+\nabla\cdot\left(\overline{\overline{\tau}}\right)+\rho\vec{g}+\vec{F} \quad (2)$$

where, μ is the dynamic viscosity (Pa s), t is the time (s), p is the pressure (Pa), $\vec{g}$ is the gravity acceleration (m s^{-2}), $\vec{F}$ is a force term (N m^{-3}), and $\overline{\overline{\tau}}$ is the stress tensor (Pa), which for an incompressible flow is written as

$$\overline{\overline{\tau}}=\mu\left(\nabla\vec{V}+\nabla\vec{V}^{T}\right) \quad (3)$$

The volume fraction equation is

$$\frac{\partial(\rho\alpha)}{\partial t}+\nabla\cdot\left(\rho\alpha\vec{v}\right)=0 \quad (4)$$

where, α is the resin volume fraction.

In Equation (2), the $\vec{F}$ term is used to include porous media flow resistance in the mathematical model. In addition, Darcy's Law.[26]

$$\vec{v}=-\frac{\overline{\overline{K}}}{\mu}\nabla p \quad (5)$$

which correlates the velocity with the pressure gradient, is used to formulate the problem. This is accomplished by recognizing in Equation (5) that the pressure gradient is actually the resistance force, and thus

$$\vec{F}=\nabla p=-\frac{\mu}{\overline{\overline{K}}}\vec{v} \quad (6)$$

where, $\overline{\overline{K}}$ is the permeability tensor (m^2).

The average physical properties are defined based on the cell volume fraction, such as in Ref. [27].

$$\rho=\alpha\rho_{\text{resin}}+(1-\alpha)\rho_{\text{air}} \quad (7)$$

$$\mu=\alpha\mu_{\text{resin}}+(1-\alpha)\mu_{\text{air}} \quad (8)$$

The thermal problem is solved by adding the energy equation to the model. In terms of temperature, can be written as

$$\frac{\partial(\rho_H c_H T)}{\partial t}+\nabla\cdot\left(\rho c T\vec{v}\right)=\nabla\cdot(k_H\nabla T) \quad (9)$$

where, c is the fluid specific heat (J kg^{-1} K^{-1}), c_H is the hybrid (reinforcement + fluid) specific heat (J kg^{-1} K^{-1}), k is the fluid conductivity (W m^{-1} K^{-1}), k_H is the hybrid conductivity (W m^{-1} K^{-1}), and T is the temperature (K).

The thermal physical properties of the fluid (air + resin) are also averaged by the cell volume fraction as follows

$$c=\alpha c_{\text{resin}}+(1-\alpha)c_{\text{air}} \quad (10)$$

$$k=\alpha k_{\text{resin}}+(1-\alpha)k_{\text{air}} \quad (11)$$

and the hybrid properties are averaged as in Ref. [28].

$$\rho_H=\left(\frac{\rho\rho_{RM}}{\rho_{RM}w+\rho(1-w)}\right) \quad (12)$$

$$c_H=cw+c_{RM}(1-w) \quad (13)$$

$$k_H=\frac{k_{RM}k}{k_{RM}w+k(1-w)} \quad (14)$$

where, subindex *RM* indicates the reinforce medium, and w is defined as

$$w=\frac{\frac{\varepsilon}{\rho}}{\frac{\varepsilon}{\rho}+\frac{1-\varepsilon}{\rho_{RM}}} \quad (15)$$

where, ε is reinforcement porosity.

Thermal and fluid flow problems are coupled to the resin viscosity dependence on time and temperature. For isothermal solutions, the resin viscosity was previously determined, and only Equations (1)–(4) must be solved. This simplification is well accepted in most solutions; however, in some cases, it is necessary to take into account temperature the variations and resin cure inside the mold cavity and thus, Equation 9 must also be solved.

Many empirical correlations are used to describe viscosity dependence with temperature and time.[1,3,19,20,22] In this work, the correlation proposed in Zhou et al.[19] for an epoxy resin, was used. This correlation was based on the dual-Arrhenius model given by

$$\mu_{\text{resin}}=1.138\times10^{-11}e^{\left(\frac{7248.5623}{T}+1.587\times10^{9}e^{\left(-\frac{7735.0037}{T}\right)}t\right)} \quad (16)$$

where, T is the temperature (K) and t is the time (s).

Another simplification compared with the solutions found in the literature is that the proposed model does not consider the energy generated from the exothermic cure [see Equation (9)] because a heat generation model based on time and temperature was not found in literature. The existing solutions are all formulated as a

function of resin conversion and cannot be used in the model proposed in this work.

2.1 | Computational modeling

A squared plate was chosen as a the computational domain for all simulations. Figure 1 shows the geometry, dimensions and inlet/outlet vents of the computational domain. In Figure 1, a is the base length (m) and h is the mold height (m).

The fluid flow boundary conditions are the prescribed pressure $p = P_0$ and resin volume fraction $\alpha = 1$ at the inlet vent, and $p = 0$ Pa and $\frac{\partial \alpha}{\partial n} = 0$ (n is the normal to the face direction) are prescribed at the outlet vents. For all other surfaces, the no slip condition and $\frac{\partial \alpha}{\partial n} = 0$ are set for the velocity and volume fraction equations, respectively.

The thermal boundary conditions are the prescribed temperatures at the inlet vent and at all mold walls. The null temperature derivative ($\frac{\partial T}{\partial n} = 0$) normal to the flow is set at outlet vents.

At the beginning of all simulations, as initial conditions, the mold is assumed to be filled only with air, at constant temperature T_0 and velocity equal to 0 m s^{-1}.

Computational domain discretization was performed with GMSH software.[29] Hexahedral elements were used in most of the grid except at the inlet and outlet vent as shown in Figure 2. The independent grid contains 154,272 volumes and was defined based on a previously performed grid independence test.[30]

The mathematical model presented in Equations (1)–(4) can be solved using the *interFoam* solver, which is the isothermal implementation of the VOF

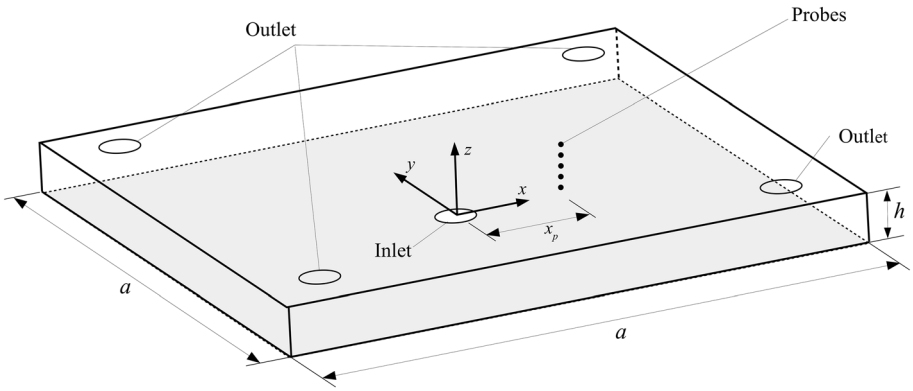

FIGURE 1 Computational domain

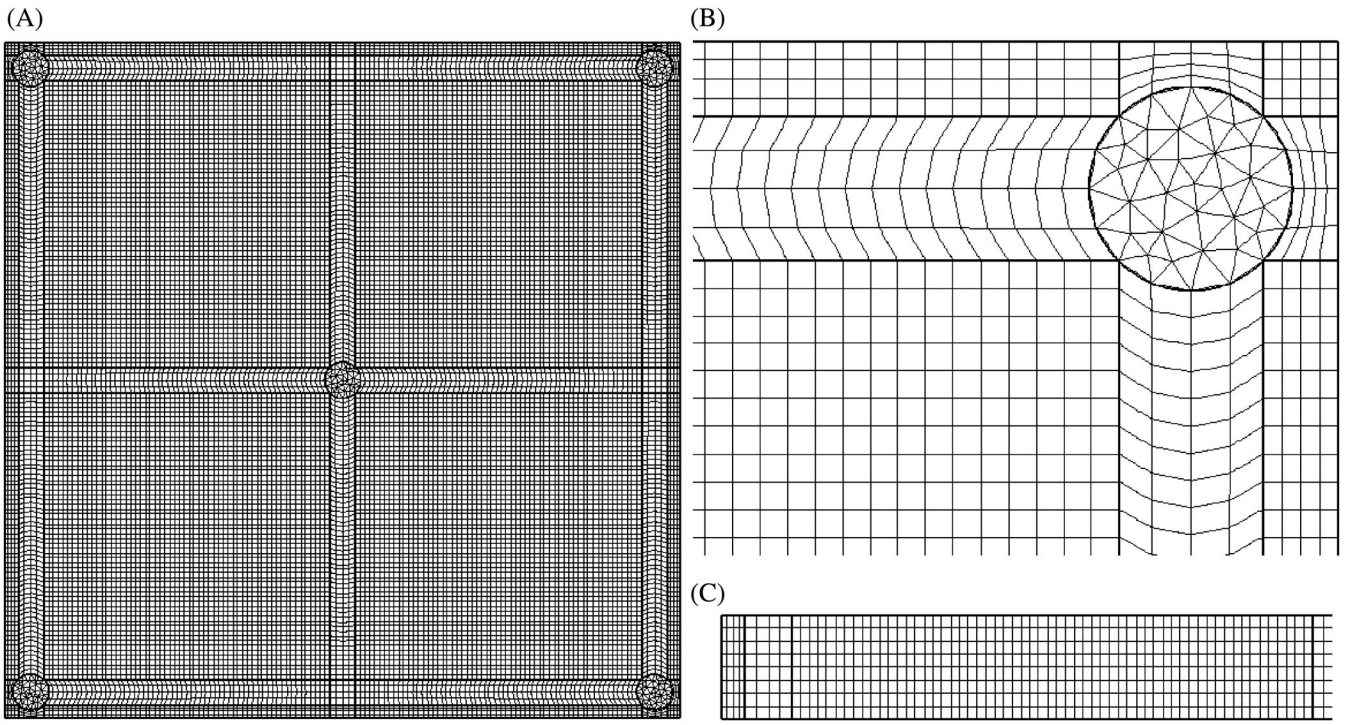

FIGURE 2 Discretization details: (A) top view, (B) outlet vent zoom, and (C) lateral view

TABLE 1 OpenFOAM control parameters

Variable	Parameter
Software version	7.0
Algorithm	PIMPLE
Solvers	
Velocity	Smooth solver
Pressure	PCG
Interpolation schemes	
Transient	Euler
Gradients	Gauss linear
Divergent	
div(phirb,alpha)	Gauss interface compression
div(rho*phi,U)	Gauss linear upwind grad(U)
div(rhoPhi,T)	Gauss linear
div(phi, alpha)	Gauss linear
div(phirb,alpha)	Gauss interface Compression limited
div((muEff*dev(T(grad (U)))))	Gauss linear
div(((rho*nuEff)*dev2(T (grad(U)))))	Gauss linear
div((rhoCp*phi),T)	Gauss upwind

method in OpenFOAM. The inclusion of the energy equation (Equation (9)) required a modification in the OpenFOAM standard solver. The modified version of *interFoam* allowed the temperature viscosity dependence to be considered. A new viscosity model, expressed by Equation (16), was also added to the OpenFoam software.

In all simulations, the Courant number (Co) was used to control the integration advance in time. According to the OpenFOAM reference manual,[31] Co for the *interFoam* solver should be no greater than 1. Thus, in the current solutions, $Co = 0.5$ was used over all of the computational domain. Other solver control parameters and discretization details are shown in Table 1.

2.2 | Thermophysical properties and process variables

All simulations presented in this work used an RTM mold with the geometry shown in Figure 1. The resin and transport medium properties were taken from Shojaei et al.,[28] and the air properties were taken from Incropera et al.[32] The physical properties and process variables used are shown in Table 2.

3 | RESULTS

Initially, an isothermal solution for the problem described in Section 2 is presented. Figure 3 shows the top and cross-sectional views for resin flow advance inside mold the cavity at $t = 30$ s. Red represents regions filled with resin ($\alpha = 1$), blue represent regions filled with air ($\alpha = 0$), and the interface between resin and air ($0 < \alpha < 1$) is represented with other colors.

In the simulation shown in Figure 3, all operating conditions were set with the values presented in Table 2. The reinforced medium is considered homogeneous with a constant in-plane permeability ($K_{xx} = K_{yy}$) that yields a radial advance in the x and y directions. These in-plane permeabilities are one order of magnitude larger than the transverse permeability (K_{zz}). The resin advance in the transverse direction depends on the $\psi = K_{xx}/K_{zz}$ ratio. If $\psi = 1$, a close to circular (the gravity effect "flattens" the flow surface) advance is also expected in the transverse direction. In the case shown in Figure 3, ψ was set to 10; thus, the expected elliptical form for resin advance can be observed (Figure 3(B)).

To better quantify the flow advance inside the mold cavity, the resin flow front was tracked along the x and z axes (see Figure 1) as a function of time. The results are shown in Figure 4 for the two studied cases with $K_{zz} = 2 \times 10^{-10}$ m^2 ($\psi = 10$) and $K_{zz} = 8 \times 10^{-12}$ m^2 ($\psi = 25$). In Figure 4, when the resin reaches the mold walls, the curves in the graph become constant. This behavior is observed in both the x and z directions only for the case with $K_{zz} = 2 \times 10^{-9}$ m^2. For the case with $K_{zz} = 8 \times 10^{-11}$ m^2, even after 450 s, the resin has not yet reached the lateral walls.

3.1 | Modified viscosity model

The solution presented in Figure 4 was obtained with the standard *interFoam* solver and constant viscosity, that is, without the inclusion of the energy equation (Equation 9) and the modified viscosity model [Equation (16)].

The first verification concerns with correct implementation of the viscosity model. To do so, the modified non-isothermal solver, named *interTempFoam*, was used to solve a constant temperature problem defined by the following thermal boundary and initial conditions: all mold walls, inlet resin temperature, and initial air temperature were set to a prescribed temperature T_0. To compare the calculated viscosity values with those obtained with Equation (16), a probe was set at coordinates (0, 0, 0). The problem described in Section 2 was solved for four different temperatures, and the viscosity was made to vary with time according to Equation (16). Figure 5 presents the viscosity variation for temperatures T_0 of 308 K

TABLE 2 Thermophysical properties and process variables

	Symbol	Value	Reference
Resin properties			
Density	ρ_{resin}	1100 kg m^{-3}	[28]
Viscosity[a]	μ_{resin}	0.45 Pa s	[28]
Specific heat	c_{resin}	1680 J kg^{-1} K^{-1}	[28]
Conductivity	k_{resin}	0.168 W m^{-1} K^{-1}	[28]
Reinforced medium properties			
Density	ρ_{RM}	2560 kg m^{-3}	[28]
Specific heat	c_{RM}	670 J kg^{-1} K^{-1}	[28]
Conductivity	k_{RM}	0.0335 W m^{-1} K^{-1}	[28]
Porosity	ε	0.6	
In-plane permeability	$K_{xx} = K_{yy}$	2×10^{-9} m^2	[28]
Transverse permeability	K_{zz}	2×10^{-10} $m^2 8 \times 10^{-11}$ m^2	
Air properties			
Density	ρ_{air}	1.1614 kg m^{-3}	[32]
Viscosity	μ_{air}	1.846×10^{-5} Pa s	[32]
Specific heat	c_{air}	1007 J kg^{-1} K^{-1}	[32]
Conductivity	k_{air}	0.0263 W m^{-1} K^{-1}	[32]
Process variables			
Inlet pressure	P_0	1 bar	
Mold dimensions			
Side length	a	0.3 m	
Height	h	0.012 m	
Inlet diameter	D_{in}	0.015 m	
Outlet diameter	D_{out}	0.015 m	

[a]For isothermal solutions.

(35°C), 313 K (40°C), 318 K (45°C), and 323 K (50°C). Direct comparison of the solution presented in Figure 5 with the results presented in Zhou et al.[19] (Equation (16)) showed good agreement.

3.2 | New solver verification and validation

The new solver, *interTempFoam*, includes the energy equation (Equation 9) in the *interFoam* solver. First, code verification was performed with an analytical solution also used by Refs. [33,34] to validate their codes. The problem consists of rectilinear injection of resin (without a reinforced medium) in a computational domain with dimensions $h \times 2\,h \times L$ ($h = 1$ m, $L = 3$ m). This problem has an analytical solution given by

$$\theta(x',y) = \sum_{n=0}^{\infty} \theta_0 \frac{2(-1)^n}{\lambda_n h} e^{-\lambda_n^2 x'} \cos(\lambda_n y) \qquad (17)$$

where, $x' = \beta \frac{x}{U}$, $\theta = T - T_{mold\ wall}$ and $\lambda_n = (2n+1)\frac{\pi}{2} h$.

Resin is injected at $T_0 = 273$ K (0°C) while the mold walls are maintained at $T_{mold\ wall} = 373$ K (100°C). The other constants in Equation (17) are the thermal diffusivity $\beta = k/(\rho\ c) = 1$ m^2 s^{-1}, the velocity $U = 1$ m s^{-1} and the mold mid-plane coordinate $y = 0$ m. The results from the analytical solution, this work and the Refs. [33,34], are compared in Figure 6, where good agreement among the different solutions can be observed. This comparison verifies the current solution for the nonisothermal case of resin and air flowing through an empty channel. However, the inclusion of the reinforced medium requires another verification run.

In sequence, code validation was carried out using the experimental results presented by Lin et al.[35] with a nonreactive fluid (palatinol oil) and glass fiber reinforcement. The laboratory experiment was performed in a circular (cylindrical) mold with an inlet radius (at center) of 0.0635 m, an outer radius of $r = 0.2$ m and thickness $W = 0.0127$ m. However, in the current numerical model, flow symmetry was considered to reduce the number of grid elements and a 30° pizza-like geometry was used.

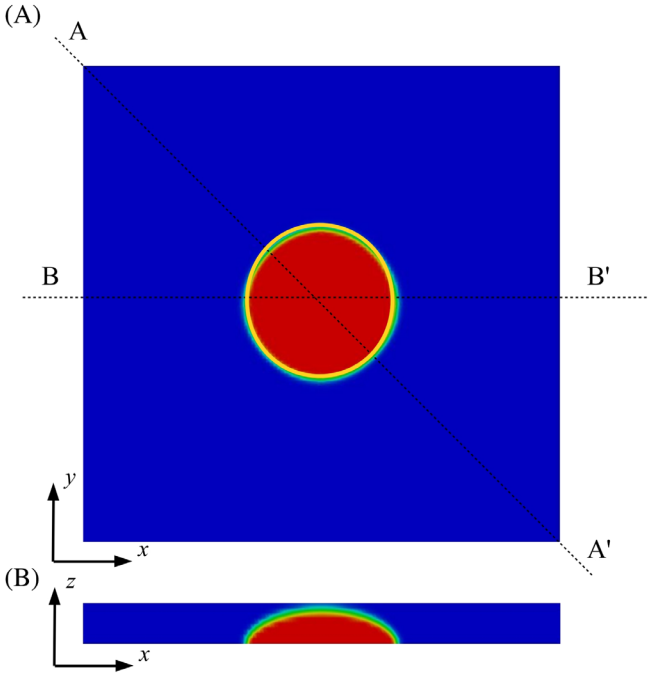

FIGURE 3 Isothermal solution at $t = 30$ s: (A) top view, (B) cross-sectional view along the B–B′ direction (not in scale) [Color figure can be viewed at wileyonlinelibrary.com]

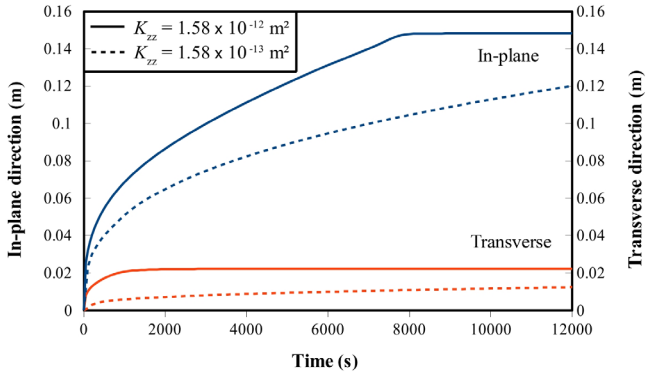

FIGURE 4 Flow position in the in-plane and transverse directions [Color figure can be viewed at wileyonlinelibrary.com]

Figure 7 presents the computational domain with geometric dimensions and boundary conditions. The fluid viscosity is temperature dependent and expressed is as

$$\mu = e^{\left(-16.376 + \frac{4125}{T}\right)} \tag{18}$$

All other thermophyscial properties of palatinol oil and reinforcement (glass fiber) are shown in Table 3.

Palatinol oil is injected with a constant flow rate of 3.4×10^{-5} m^3 s^{-1} (2.833×10^{-6} m^3 s^{-1} in the 30° computational domain of Figure 7) at the inlet vent. The top and bottom walls are held at a constant temperature of 348 K (75°C), symmetric boundary conditions are applied

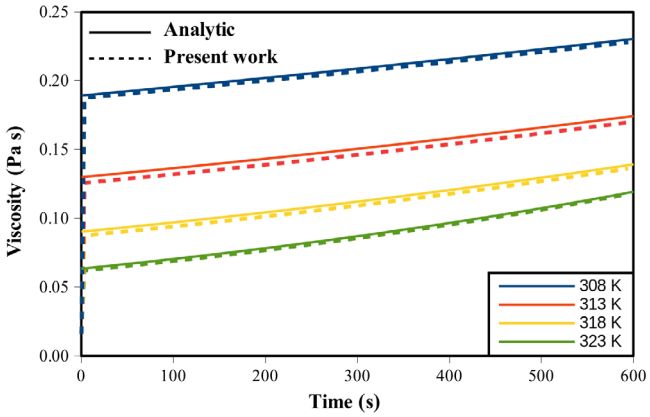

FIGURE 5 Verification of the viscosity time dependence solution [Color figure can be viewed at wileyonlinelibrary.com]

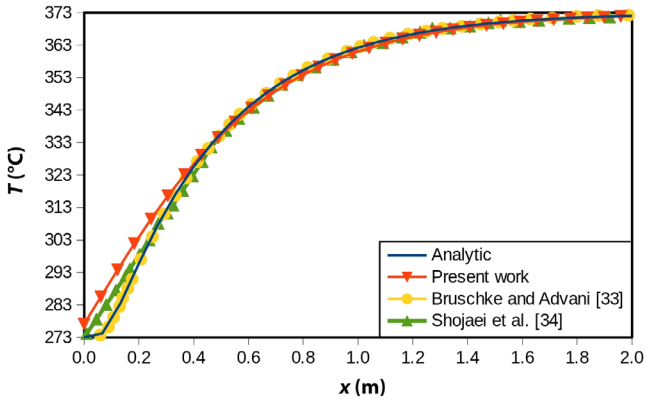

FIGURE 6 Verification of the thermal solution [Color figure can be viewed at wileyonlinelibrary.com]

to the sidewalls and fully developed flow is set to the outlet vent. At the beginning of the simulation, the mold is filled only with air at 348 K (75°C).

The temperature is tracked with two probes positioned 0.04 and 0.08 m away from the mold center (see Figure 7). These probes are placed exactly at the midplane between bottom the and top walls. Temperature is measured as a function of time, and the results are plotted in Figure 8. Figure 8 also plots the experimental results reported in Lin et al.[35] and the numerical results of Tan and Pillai.[36] For both probe locations, the results from this work predicted that the temperature starts to drop almost at the same time reported experimentally in Ref. [35]; however, the temperature drops much faster in the numerical simulation. The lowest temperatures for probes 1 and 2 are reached at approximately at 11 and 26 s in the experimental run and at 4 and 14 s in the numerical solution, respectively. The simulated lowest temperature is 293.1 K (20.1°C), approximately 1 degree lower than the experimental results.

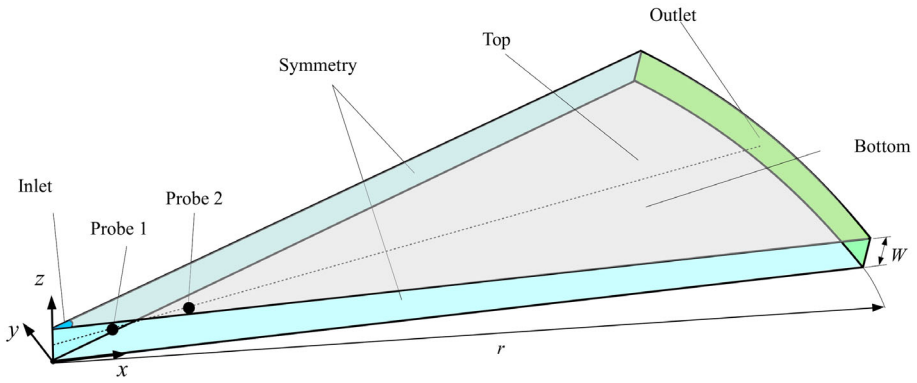

FIGURE 7 Nonreactive and nonisothermal model verification [Color figure can be viewed at wileyonlinelibrary.com]

TABLE 3 Thermophysical properties of palatinol oil and reinforcement[35]

	ρ (kg m^{-3})	c_p (J kg^{-1} k^{-1})	k (W m^{-1} k^{-1})	K (m^2)	ε	μ (Pa s)
Palatinol oil	0.98	1.62	0.135	–	–	–
Reinforcement	2.56	670	0.67	3.4×10^{-9}	0.8	Equation (18)

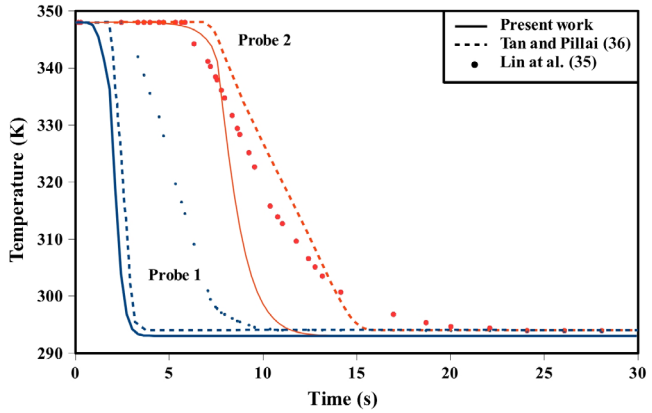

FIGURE 8 Nonreactive solver verification and validation [Color figure can be viewed at wileyonlinelibrary.com]

From comparison of current the solution with the numerical results presented in Ref. [36], different degrees of agreement were observed for the probe 1 and probe 2 temperature profiles. In both numerical solutions, at the probe 1 location, a rapid temperature drop is observed, with the current solution always approximately 1 degree lower. At probe location 2, the same rapid temperature drop is predicted in the current solution, but the results reported in Ref. [36] presented an unexpectedly (compared with the probe 1 temperature profile) smoother temperature drop, which better agrees with the experimental results of Ref. [35].

Even though differences are observed between the current solution and the results reported in the literature, two important parameters are correctly predicted: the instant when the temperature starts to decrease and the overall temperature drops. However, the simulated temperature profiles are not in good quantitative agreement with the experimental runs in terms of the time needed to reach the lowest temperature, which is longer in the experimental results reported in Ref. [35]. Despite these minor differences, it is possible to infer that in a general way the proposed computational model was verified and validated.

3.3 | Comparison with the conversion-based model

This simulation compares the proposed model (in which resin viscosity is a function of time and temperature) with the widely accepted standard model (which correlates resin viscosity with temperature and conversion). Figure 9 describes the mold geometry and boundary conditions for a problem studied in the work of Shojaei et al.[34] At the inlet vent, the resin flow rate is fixed to 5.5×10^{-6} m^3 s^{-1}, and the temperature is 293 K (20°C). Atmospheric pressure and a zero gradient in the flow direction are prescribed for fluid and thermal problems, respectively, at the outlet vent. All other boundaries are walls (no slip) with a constant temperature of 348 K (75°C). The simulation begins with the mold filled with air at 348 K (75°C).

The viscosity model proposed by Ref. [34] is given by

$$\mu = \mu_0 e^{\left(\frac{E_\mu}{RT}\right)} \left[\frac{\alpha_g}{\alpha_g - \alpha}\right]^{(A+B\alpha)} \tag{19}$$

where, $A = 1.5$ and $B = 1$ are nondimensional constants, μ_0 is a reference viscosity (2.78×10^{-4} Pa s), E_μ is the

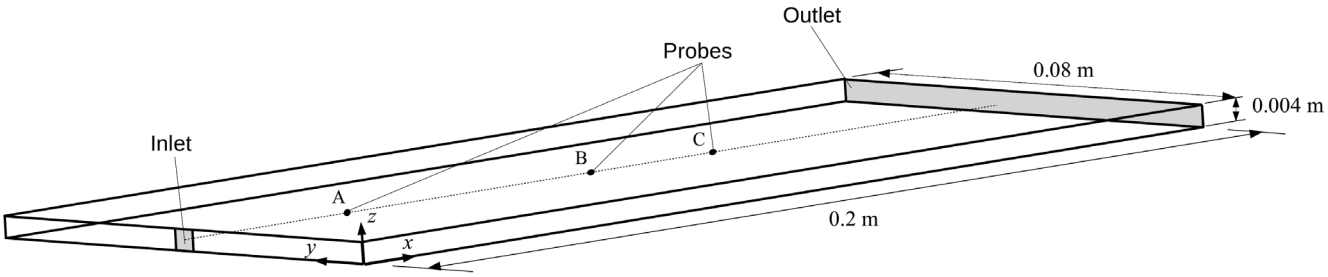

FIGURE 9 Reactive solver solution [Color figure can be viewed at wileyonlinelibrary.com]

activation energy (18,000 J mol^{-1}), R is the universal gas constant (8314 J/mol K^{-1}), α is the conversion, and $\alpha_g = 0.1$ is the conversion at the gel point.

Three probes are used to track temperature changes as a function of time. The probes are positioned at coordinates A (0.04 m, 0.04 m, 0.02 m), B (0.1 m, 0.04 m, 0.02 m), and C (0.13 m, 0.04 m, 0.02 m) as shown in Figure 9.

The viscosity correlation expressed by Equation (19) cannot be exactly reproduced with the mathematical model proposed in this work; it is a function of temperature and conversion, but the viscosity correlation used here in this work (Equation (16)) is a function of temperature and time. It is important to highlight that this is not a verification of the proposed solution but a comparison with a widely accepted model reported several times in the literature. Thus, Equation (19) is simplified by setting the term $(\alpha_g/[\alpha_g - \alpha])$ equal to 1, that is, the effect of conversion to viscosity was neglected.

Another important difference exists between the flow model used in this work and the one used in the work of Shojaei et al.[34] In this work, the VOF[23] multiphase model is used to determine the flow behavior of both air and resin, whereas in Ref. [34], the control volume finite element method (CV/FEM),[12] which accounts only for the resin flow, was employed.

The temperature profiles of the current simulation and the results presented by Ref. [34] are shown in Figure 10. Initially, at the probe locations, only air and temperature remain unchanged up to the moment that the resin approaches. Because the temperature is lower in the resin than in the air (due to the imposed boundary conditions), when resin passes through the probe locations, the temperature begins to drop, and the observed profiles are plotted in Figure 10.

The first point to be analyzed in Figure 10 is the moment when the temperature starts to drop. In the two-phase model proposed in this work, this moment occurs very close to the instant when the resin reaches the probe location (t_A, t_B, and t_C in Figure 10), whereas in Ref. [34], the temperature starts to drop much earlier, indicating

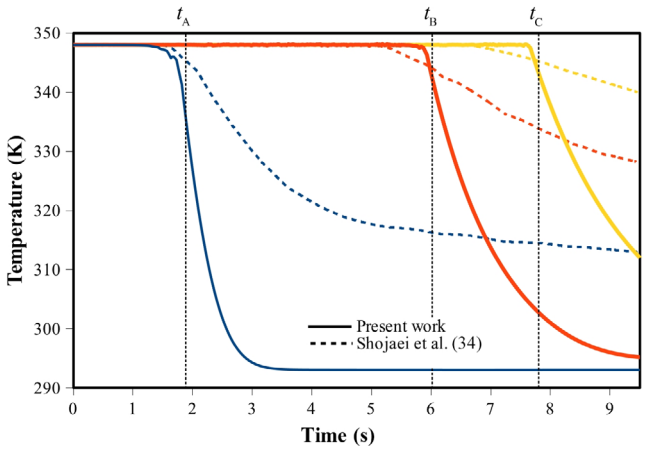

FIGURE 10 Comparison between the proposed model and conversion-based model [Color figure can be viewed at wileyonlinelibrary.com]

that in the two-phase model, energy takes longer to be transferred from the air to the resin. The second analysis is related to the overall temperature drop, which is much faster in the proposed method than in the results presented in Ref. [34]. This observation is due to a simplification in the current solution that does not include heat generation during the curing process. In all models found in the literature, heat generation due to the curing process is formulated in the energy equation as a function of conversion. Unfortunately, the main simplification proposed in this work is not designed to solve this transport equation. Thus, it could be necessary to find, or develop, a heat generation term described as a function of temperature and time, which is not the objective of this work.

3.4 | Nonisothermal simulation

For the nonisothermal simulation, the new solver (*interTempFoam*) was used to solve the full problem described in Section 2 by Equations (1)–(4) and (9). The constitutive equations for the model are given by Equations (6)–(8)

and (10)–(16). The problem is fully coupled because viscosity depends on temperature; thus, the flow equations are temperature dependent, and the energy equation depends on the velocity field.

This case study is described with the computational domain shown in Figure 1. The geometry dimensions, boundary conditions and physical properties are presented in Table 2. The thermal problem was defined by considering the initial air temperature at 308 K (35°C), resin entering the mold at 308 K (35°C), bottom mold wall at 323 K (50°C), top mold wall at 308 K (35°C) and insulated lateral walls. At the outlet vent, a null temperature derivative was set in the flow direction.

Figure 11 shows the flow advance, temperature and viscosity profiles at t = 5, 10, 50, 100, 150, and 200 s for a cross-sectional cut along direction A–A′ (see Figure 3).

From Figure 11(A) and (B), it can be observed that cold resin at 308 K (35°C) is forced through a heated (bottom wall) mold. The resin flows up for approximately t = 175 s before it starts to leave the mold through the outlet vents. The viscosity profiles for the same time instants are shown in Figure 11(C). Throughout the entire injection time, the temperatures inside the resin region and adjacent areas are lower, similar to its inlet value of 308 K (35°C). In the regions not yet occupied by resin, that is, with air only, a nearly linear temperature gradient is observed from the lower bottom wall at 323 K (50°C) toward the upper mold wall at 308 K (35°C). The last plots (for t = 200 s) in Figure 11 represent a steady-state condition in which the temperature and viscosity profiles no longer change. Due to the lower temperature boundary condition applied to the top wall and inlet vent, a temperature gradient is observed from the bottom mold wall (higher temperature) to the top mold wall (lower temperature). As viscosity decreases with increasing temperature, a viscosity gradient is also observed between

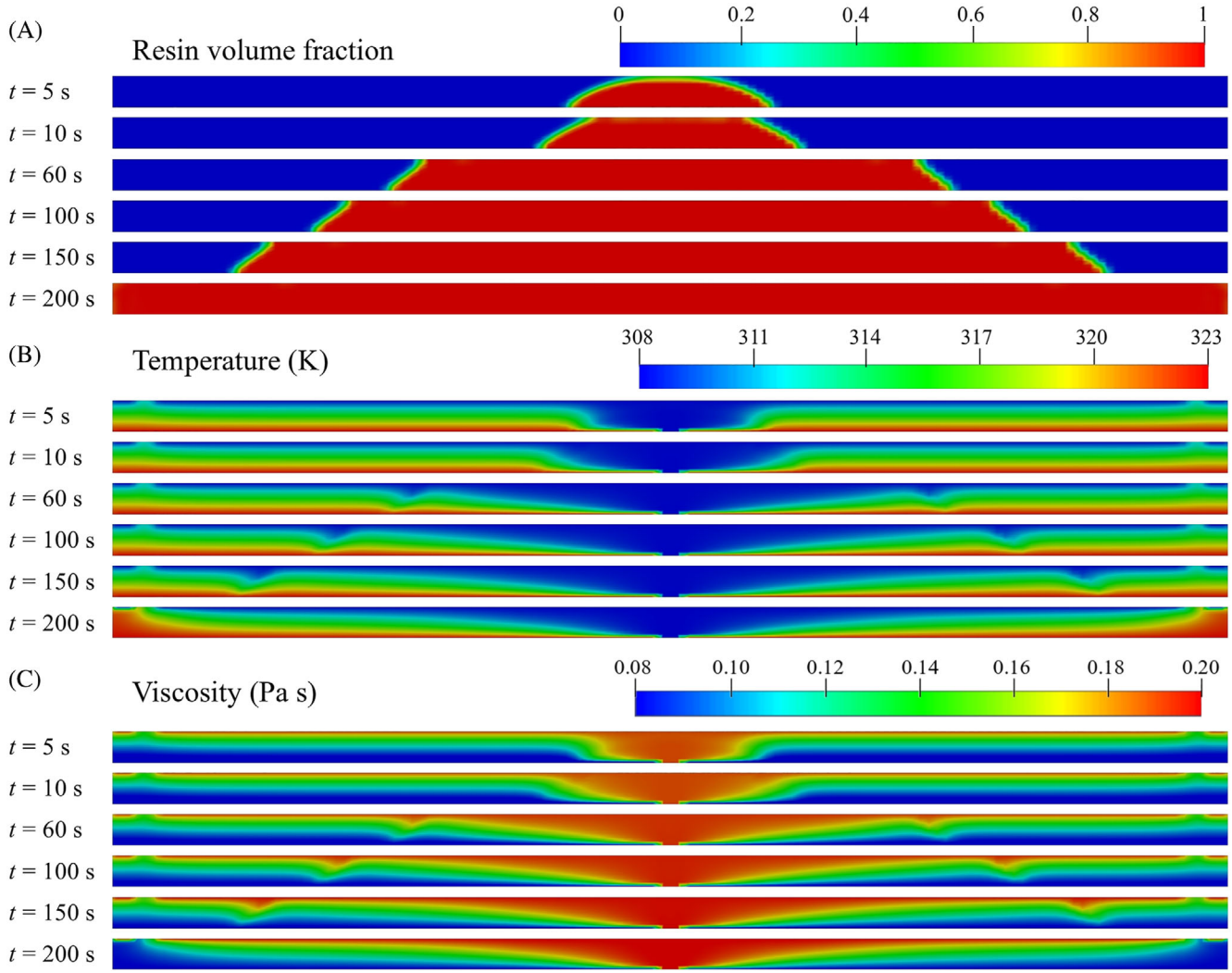

FIGURE 11 Resin cross-section profiles along the A–A′ direction (see Figure 3) as a function of time: (A) flow position, (B) temperature, and (C) viscosity [Color figure can be viewed at wileyonlinelibrary.com]

the bottom and top mold walls; however, the viscosity has a larger value close to the cold (top) mold wall. A time influence also exists on the resin viscosity, but its effect is small compared with the temperature effect (see Figure 5) and cannot be observed in Figure 11.

Temperature and viscosity were also investigated along the transverse (z) direction. Five probes positioned at coordinates $x_p = 0.05$ m, $y_p = 0.0$ m, and $z_p = 0.002$ m, 0.004 m, 0.006 m, 0.008 m, and 0.010 m (see Figure 1) were used to track temperature and viscosity changes with time as shown in Figures 12 and 13. At the beginning, only air is present at the probe locations (cold resin has not reached the probes), and a quick increase in temperature is observed. Subsequently, when the resin approaches the probes, the temperature starts to drop and stabilizes a few seconds later at a lower value, which remains constant during the entire injection process. At approximately 175 s, resin reaches the outlet vents and a steady-state condition is achieved for fluid flow. However, the temperature fields are not yet stabilized, and a small increase in the temperature profiles can be observed after this time. The temperature profiles finally enter the steady state condition approximated at 200 s. During the injection time, between 40 and 160 s, the temperature profiles are almost constant with time and vary in the transverse direction from approximately 315 K (42°C) at $z = 0.002$ m (closest to the heated wall probe), to 308.5 K (35.5°C) at $z = 0.01$ m (closest to the cold wall probe).

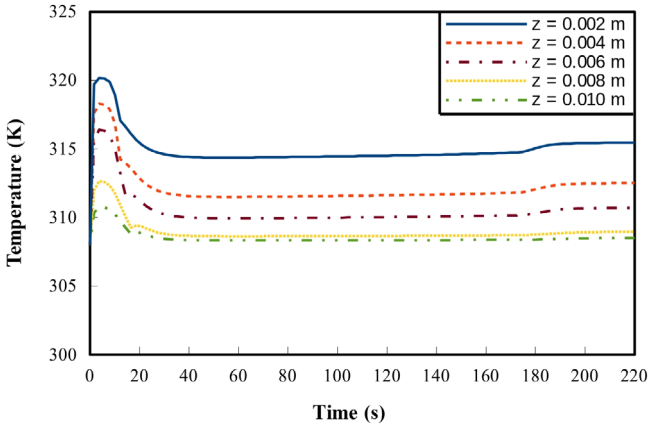

FIGURE 12 Temperature variations along the transverse (z) direction at $x = 0.05$ m and $y = 0.0$ m [Color figure can be viewed at wileyonlinelibrary.com]

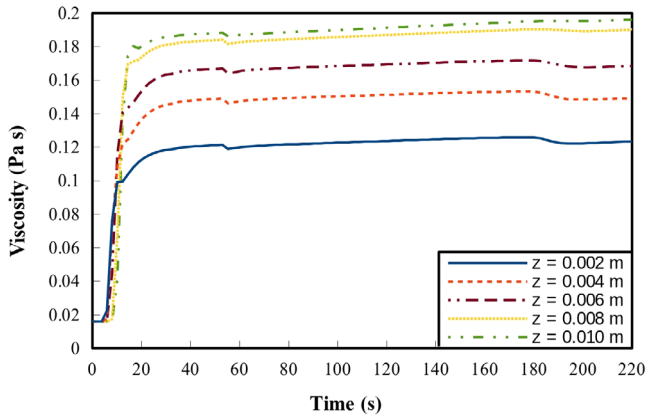

FIGURE 13 Viscosity changes variations along the transverse (z) direction at $x = 0.1$ m and $y = 0.0$ m [Color figure can be viewed at wileyonlinelibrary.com]

The viscosity profiles along the transverse direction (see probe locations in Figure 1) are shown in Figure 13. Before any interpretation of the results presented in Figure 13, it is important to remember that in the current model, the fluid physical properties are averaged with the resin volume fraction α at every finite volume in the computational domain. This has no effect in regions far from the two-fluid interface but strongly affects all physical properties at the resin flow front. At the beginning, when only air is present at the probe locations, the flow viscosity plotted in Figure 13 is actually the air viscosity (1.45×10^{-5} Pa s). During the period of time when the flow front passes by the probes, the flow viscosity is averaged between the air viscosity and resin viscosity calculated with Equation (16) (at 308 K [35°C], $\mu_{resin} = 0.189$ Pa s). Subsequently, the resin is calculated only with Equation (16). Thus, it is possible to explain the quick change in viscosity presented in Figure 13 between 5 and 20 s. The temperature peaks observed in Figure 12 do not result in a viscosity decrease in the profiles of Figure 13 because at this period of time, only air is present at the probe locations. During the time period with constant temperature profiles shown in Figure 12, a very small change (increase) in viscosity is observed in Figure 13. This increase is due to time effects (see Equation (16)), which are not significant for small injection times and are almost unperceptible in Figure 13 for this reason. However, the temperature change at the final instants of the injection process is clearly observed as a small decrease in the viscosity profiles in Figure 13.

4 | CONCLUSIONS

Numerical simulations of resin injection in RTM and similar liquid molding processes have been largely explored in the literature. Most of existing work found assumed an isothermal condition in which all physical properties, including viscosity, are kept constant. This simplification may be adequate in many cases; however, situations exist in which where the dependence of viscosity on time and temperature must be considered, such as

in the processing of thick parts with low injection pressure or high fiber content.

In this work, OpenFOAM software was used to simulate the resin advance inside the mold cavity. The standard solver *interFoam* did not account for the thermal solution or viscosity dependence on temperature and time, and thus a new solver had to be compiled in which transport equations for volume fraction, momentum, continuity and energy form a fully coupled system of differential partial equations. The new solver, called *interTempFoam*, was tested with three verification and/or validation cases.

The new solver was used to explore the viscosity influence on the flow advance inside the mold cavity. The results showed that both variables are important and must be carefully controlled. At the beginning of resin injection, temperature is the determining parameter that defines viscosity, and the higher the temperature, the lower the viscosity, which is beneficial because the overall injection process is faster. However, with higher temperatures, the gelation/cure effects take place sooner, and depending on the particular conditions, such as mold size and reinforcement permeability, complete mold filling may not be achieved because resin flow is prevented. Based on the satisfactory results obtained with the computational model presented in this article, future work will improve the model with the inclusion of heat generation during the curing process.

ACKNOWLEDGMENTS

The authors thank Conselho Nacional de Desenvolvimento Científico e Tecnológico (CNPq), Coordenação de Aperfeiçoamento de Pessoal de Nível Superior-Brasil (CAPES)-Finance Code 001, and Fundação de Amparo à Pesquisa do Estado do Rio Grande do Sul (FAPERGS) for funding and for encouraging innovation and research in Brazil and abroad.

ORCID

Laisa Luiz Soares https://orcid.org/0000-0003-3353-6381
Sandro Campos Amico https://orcid.org/0000-0003-4873-2238
Liércio André Isoldi https://orcid.org/0000-0002-9337-3169
Jeferson Avila Souza https://orcid.org/0000-0002-6987-8263

REFERENCES

[1] C. Garschke, P. P. Parlevliet, C. Weimer, B. L. Fox, *Polym. Test.* **2013**, *32*, 150. https://doi.org/10.1016/j.polymertesting.2012.09.011.
[2] A. Yousefi, P. G. Lafleur, R. Gauvin, *Polym. Compos.* **1997**, *18*, 157. https://doi.org/10.1002/pc.10270.
[3] X. Yi, X. Kuang, L. Kong, X. Dong, Z. Feng, D. Wang, *J. Appl. Polym. Sci.* **2017**, *134*, 45282. https://doi.org/10.1002/app.45282.
[4] R. Agogue, N. Chebil, M. Deleglise-Lagardere, P. Beauchene, C. H. Park, *Appl. Compos. Mater.* **2018**, *25*, 1169. https://doi.org/10.1007/s10443-017-9659-8.
[5] W. Changchun, B. Guanghui, W. Yang, Z. Boming, P. Lijian, *Appl. Compos. Mater.* **2015**, *22*, 363. https://doi.org/10.1007/s10443-014-9412-5.
[6] F. V. Härter, J. A. Souza, L. A. Isoldi, E. D. Santos, S. C. Amico, *Matéria (Rio de Janeiro)*. **2017**, *22*. https://doi.org/10.1590/s1517-707620170002.0167.
[7] N. Vernet, F. Trochu, *J. Compos. Mater.* **2016**, *50*, 1951. https://doi.org/10.1177/0021998315597989.
[8] D. May, A. Aktas, S. G. Advani, D. C. Berg, A. Endruweit, E. Fauster, S. V. Lomov, A. Long, P. Mitschang, S. Abaimov, D. Abliz, I. Akhatov, M. A. Ali, T. D. Allen, S. Bickerton, M. Bodaghi, B. Caglar, H. Caglar, A. Chiminelli, N. Correia, B. Cosson, M. Danzi, J. Dittmann, P. Ermanni, G. Francucci, A. George, V. Grishaev, M. Hancioglu, M. A. Kabachi, K. Kind, M. Deléglise-Lagardère, M. Laspalas, O. V. Lebedev, M. Lizaranzu, P.-J. Liotier, P. Middendorf, J. Morán, C.-H. Park, R. B. Pipes, M. F. Pucci, J. Raynal, E. S. Rodriguez, R. Schledjewski, R. Schubnel, N. Sharp, G. Sims, E. M. Sozer, P. Sousa, J. Thomas, R. Umer, W. Wijaya, B. Willenbacher, A. Yong, S. Zaremba, G. Ziegmann, *Compos. Part A: Appl. Sci. Manuf.* **2019**, *121*, 100. https://doi.org/10.1016/j.compositesa.2019.03.006.
[9] L. A. Isoldi, C. P. Oliveira, L. A. O. Rocha, J. A. Souza, S. C. Amico, *J. Braz. Soc. Mech. Sci. Eng.* **2012**, *34*, 105. https://doi.org/10.1590/S1678-58782012000200001.
[10] C. P. Oliveira, J. A. Souza, L. A. Isoldi, S. C. Amico, *J. Reinf. Plast. Compos.* **2013**, *32*, 3.
[11] M. V. Bruschke, S. G. Advani, A. Finite-Element Control, *Polym. Compos.* **1990**, *11*, 398.
[12] F. R. Phelan, *Polym. Compos.* **1997**, *18*, 460.
[13] F. Shi, X. Dong, *Finite Elem. Anal. Des.* **2011**, *47*, 764. https://doi.org/10.1016/j.finel.2011.02.007.
[14] A. Saad, A. Echchelh, M. Hattabi, M. El Ganaoui, *J. Reinf. Plast. Compos.* **2012**, *31*, 1388. https://doi.org/10.1177/0731684412458166.
[15] A. Saad, A. Echchelh, M. Hattabi, M. El Ganaoui, An optimized control volume/finite element method (CV/FEM) for non-isothermal liquid composite molding (LCM) process. in *Thermo-Mechanics Applications and Engineering Technology* (Eds: Z. Driss, B. Necib, H.-C. Zhang), Springer International Publishing, Cham **2018**, p. 81.
[16] A. Abbassi, M. R. Shahnazari, *Appl. Therm. Eng.* **2004**, *24*, 2453. https://doi.org/10.1016/j.applthermaleng.2004.03.005.
[17] A. Skordos, I. Partridge, Monitoring and heat transfer modelling of the cure of thermoset composites processed by resin transfer moulding (RTM). In: Polym. Compos. Int. Symp. Polym. Compos. Sci. Technol., **1999**, 223+.
[18] V. Antonucci, M. Giordano, K.-T. Hsiao, S. G. Advani, *Int. J. Heat Mass Transfer* **2002**, *45*, 1675. https://doi.org/10.1016/S0017-9310(01)00266-6.

[19] Z. Zhou, B. Jiang, X. Chen, F. Jiang, Y. Jian, *J. Wuhan Univ. Technol.-Mater. Sci. Ed.* **2014**, *29*, 1078. https://doi.org/10.1007/s11595-014-1046-9.

[20] S. Caba, M. Koch, *AIP Conf. Proc.* **2016**, 070002. https://doi.org/10.1063/1.4965534.

[21] M. B. Roller, *Polym. Eng. Sci.* **1975**, *15*, 406. https://doi.org/10.1002/pen.760150603.

[22] H. Li, B. Zhang, *Polym. Eng. Sci.* **2016**, *56*, 617. https://doi.org/10.1002/pen.24286.

[23] C. W. Hirt, B. D. Nichols, *J. Comput. Phys.* **1981**, *39*, 201. https://doi.org/10.1016/0021-9991(81)90145-5.

[24] E. Poodts, G. Minak, L. Mazzocchetti, L. Giorgini, *Compos. Part B: Eng.* **2014**, *56*, 673. https://doi.org/10.1016/j.compositesb.2013.08.088.

[25] M. Deléglise, P. Le Grognec, C. Binetruy, P. Krawczak, B. Claude, *Compos. Part A: Appl. Sci. Manuf.* **2011**, *42*, 1390. https://doi.org/10.1016/j.compositesa.2011.06.002.

[26] C. D. Rudd, A. C. Long, K. N. Kendall, C. Mangin, *Liquid Moulding Technologies: Resin Transfer Moulding., Structural Reaction Injection Moulding and Related Processing Techniques*, Woodhead Publishing Limited, Abington Cambridge, England **1997**.

[27] V. Srinivasan, A. J. Salazar, K. Saito, *Appl. Math. Model.* **2011**, *35*, 3710.

[28] A. Shojaei, S. Ghaffarian, S. Karimian, *Compos. Struct.* **2004**, *65*, 381. https://doi.org/10.1016/j.compstruct.2003.12.001.

[29] C. Geuzaine, J.-F. Remacle, *Int. J. Numer. Methods Eng.* **2009**, *79*, 1309. https://doi.org/10.1002/nme.2579.

[30] L.L. Soares. Simulação Numérica do Processo de RTM para a Infiltração de Reforços Espessos Considerando a Variação da Viscosidade da Resina em Função da Temperatura e do Tempo, Master Thesis, Universidade Federal do Rio Grande - FURG, **2016**. https://argo.furg.br/bin/bdtd/tde_busca/arquivo.php?codArquivo=11509

[31] H. Weller, C. Greenshields, C. de Rouvray, The OpenFOAM Foundation Ltd, OpenFOAM. (n.d.). https://openfoam.org/

[32] F. P. Incropera, D. P. DeWitt, T. L. Bergman, A. S. Lavine, *Fundamentals of Heat and Mass Transfer*, 6th ed., John Wiley & Sons, Hoboken, NJ **2007**.

[33] M. V. Bruschke, S. G. Advani, *Int. J. Numer. Methods Fluids* **1994**, *19*, 575.

[34] A. Shojaei, S. R. Ghaffarian, S. M. H. Karimian, *Compos. Sci. Technol.* **2003**, *63*, 1931.

[35] R. J. Lin, L. J. Lee, M. J. Liou, *Polym. Compos.* **1993**, *14*, 71.

[36] H. Tan, K. M. Pillai, *Int. J. Heat Mass Transfer* **2010**, *53*, 2256.

How to cite this article: Soares LL, Amico SC, Isoldi LA, Souza JA. Modeling of the resin transfer molding process including viscosity dependence with time and temperature. *Polymer Composites*. 2021;42:2795–2807. https://doi.org/10.1002/pc.26014